

Multiquark states in the covariant quark confinement model

Mikhail A. Ivanov*

JINR

E-mail: ivanovm@theor.jinr.ru

This talk reviews the last applications of the covariant quark model for studying the properties of the multiquark states: B_s -meson (quark-antiquark state), light baryons (three-quark states) and tetraquark (four-quark state). The form factors of the $B(B_s) \rightarrow P(V)$ -transitions are evaluated in the full kinematical region of momentum transfer squared. The widths of some B_s -nonleptonic decays are calculated. The static properties of the proton and neutron, and the Λ -hyperon (magnetic moments and charge radii) and the behavior of the nucleon form factors at low momentum transfers are described. The consequences of treating the $X(3872)$ meson as a tetraquark bound state are explored. The decay widths of the observed channels $X \rightarrow J/\psi + 2\pi(3\pi)$ and $X \rightarrow \bar{D}^0 + D^0 + \pi^0$ via the intermediate off-shell states $X \rightarrow J/\psi + \rho(\omega)$ and $X \rightarrow \bar{D} + D^*$ are calculated. Its one-photon decay $X \rightarrow \gamma + J/\psi$ is also analyzed.

*XXI International Baldin Seminar on High Energy Physics Problems,
September 10-15, 2012
JINR, Dubna, Russia*

*Speaker.

1. Introduction

The covariant quark model with infrared confinement developed in a series of papers (see Refs. [1]-[5]) is a successful tools for a unified description of the multiquark states: mesons, baryons, tetraquarks, etc. The covariant quark model is an effective quantum field approach to hadronic interactions based on the interaction Lagrangian between hadrons and their constituent quarks. Knowing a corresponding interpolating quark current allows calculating the matrix element of physical processes in a consistent way. A distinctive feature of this approach is that the multiquark states, such as baryons (three quarks), tetraquarks (four quarks), etc., can be considered and described as rigorously as the simplest quark-antiquark systems (mesons). The coupling constants between hadrons and their interpolating quark currents are determined from the connection condition $Z_H = 0$ proposed in Refs. [6, 7] and used further in numerous subfields of particle physics (for a review, see Refs. [8, 9, 10]). Here Z_H is a renormalization constant of the hadron wave function. The matrix elements of physical processes are determined by a set of associated quark diagrams, which are constructed according to $1/N_c$ -expansion. In the covariant quark model an infrared cutoff is effectively introduced in the space of Fock-Schwinger parameters, which are integrated out in the expressions for the matrix elements. Such a procedure allows one to eliminate all the threshold singularities associated with quark production and thereby ensures quark confinement. The model has no ultraviolet divergences due to vertex hadron-quark form factors, which describe a nonlocal structure of hadrons. The covariant quark model has a few free parameters: a mass of constituent quarks, an infrared cutoff parameter that characterizes confinement region, and parameters that describe an effective size of hadrons.

We review here the last applications of the covariant quark model for studying the properties of the B_s -meson, the light baryons and tetraquarks. The form factors of the $B(B_s) \rightarrow P(V)$ -transitions are evaluated in the full kinematical region of momentum transfer squared. As an application of the obtained results the widths of the B_s -nonleptonic decays are calculated. The modes $D_s^- D_s^+$, $D_s^{*-} D_s^+ + D_s^- D_s^{*+}$ and $D_s^{*-} D_s^{*+}$ give the largest contribution to $\Delta\Gamma$ for the $B_s - \bar{B}_s$ system. The mode $J/\psi\phi$ is suppressed by the color factor but it is interesting for the search of CP-violating New-Physics possible effects in the $B_s - \bar{B}_s$ mixing.

The static properties of the proton and neutron, and the Λ -hyperon (magnetic moments and charge radii) and the behavior of the nucleon form factors at low momentum transfers are described. The conservation of gauge invariance of the electromagnetic transition matrix elements in the presence of a nonlocal coupling of the baryons to the three constituent quark fields is discussed.

The consequences of treating the X(3872) meson as a tetraquark bound state are explored. The decay widths of the observed channels $X \rightarrow J/\psi + 2\pi(3\pi)$ and $X \rightarrow \bar{D}^0 + D^0 + \pi^0$ via the intermediate off-shell states $X \rightarrow J/\psi + \rho(\omega)$ and $X \rightarrow \bar{D} + D^*$ are calculated. Its one-photon decay $X \rightarrow \gamma + J/\psi$ is also analyzed. The matrix element of the transition $X \rightarrow \gamma + J/\psi$ is calculated and its gauge invariance is proved. For reasonable values of the size parameter Λ_X of the X(3872) consistency with the available experimental data is found. The possible impact of the X(3872) in a s-channel dominance description of the J/ψ dissociation cross section is discussed.

2. Covariant quark model

The coupling of a hadron H to its constituent quarks is described by the Lagrangian:

$$\mathcal{L}_{\text{int}} = g_H \cdot H(x) \cdot J_H(x) \quad (2.1)$$

where the quark currents are defined as

$$\begin{aligned} J_M(x) &= \int dx_1 \int dx_2 F_M(x, x_1, x_2) \cdot \bar{q}_{f_1}^a(x_1) \Gamma_M q_{f_2}^a(x_2) && \text{Meson} \\ J_B(x) &= \int dx_1 \int dx_2 \int dx_3 F_B(x, x_1, x_2, x_3) \\ &\quad \times \Gamma_1 q_{f_1}^{a_1}(x_1) \left(q_{f_2}^{a_2}(x_2) C \Gamma_2 q_{f_3}^{a_3}(x_3) \right) \cdot \varepsilon^{a_1 a_2 a_3} && \text{Baryon} \\ J_T(x) &= \int dx_1 \dots \int dx_4 F_T(x, x_1, \dots, x_4) \\ &\quad \times \left(q_{f_1}^{a_1}(x_1) C \Gamma_1 q_{f_2}^{a_2}(x_2) \right) \cdot \left(\bar{q}_{f_3}^{a_3}(x_3) \Gamma_2 C \bar{q}_{f_4}^{a_4}(x_4) \right) \cdot \varepsilon^{a_1 a_2 c} \varepsilon^{a_3 a_4 c} && \text{Tetraquark} \end{aligned}$$

where Γ is a Dirac matrix or a string of Dirac matrices which projects onto the spin quantum number of the hadron $H(x)$. The matrix $C = \gamma^0 \gamma^2$ is the usual charge conjugation matrix and the a_i ($i = 1, 2, 3$) are color indices. The function F_H is related to the scalar part of the Bethe-Salpeter amplitude and characterizes the finite size of the hadron. To satisfy translational invariance the function F_H has to fulfil the identity $F_H(x+a, x_1+a, \dots, x_n+a) = F_H(x, x_1, \dots, x_n)$ for any four-vector “a”. In the following we use a specific form for the scalar vertex function

$$F_H(x, x_1, \dots, x_n) = \delta \left(x - \sum_{i=1}^n w_i x_i \right) \Phi_H \left(\sum_{i < j} ((x_i - x_j)^2) \right), \quad (2.2)$$

where Φ_H is the correlation function of the constituent quarks with masses m_i , ($i = 1, \dots, n$) and the mass ratios $w_i = m_i / \sum_{j=1}^n m_j$.

The coupling constant g_H in Eq. (2.1) is determined by the so-called *compositeness condition* originally proposed in Refs. [6, 7] and extensively used in Refs. [8, 9, 10]. The compositeness condition requires that the renormalization constant of the elementary hadron field $H(x)$ is set to zero

$$Z_H = 1 - g_H^2 \Pi'_H(m_H^2) = 0 \quad (2.3)$$

where Π'_H is the derivative of the hadron mass operator. To clarify the physical meaning of the compositeness condition in Eq. (2.3), we first want to remind the reader that the renormalization constant $Z_H^{1/2}$ can also be interpreted as the matrix element between the physical and the corresponding bare state. The condition $Z_H = 0$ implies that the physical state does not contain the bare state and is appropriately described as a bound state. The interaction Lagrangian of Eq. (2.1) and the corresponding free parts of the Lagrangian describe both the constituents (quarks) and the physical particles (hadrons) which are viewed as the bound states of the quarks. As a result of the interaction, the physical particle is dressed, i.e. its mass and wave function have to be renormalized. The

condition $Z_H = 0$ also effectively excludes the constituent degrees of freedom from the space of physical states. It thereby guarantees that there is no double counting for the physical observable under consideration. The constituents exist only in virtual states. One of the corollaries of the compositeness condition is the absence of a direct interaction of the dressed charged particle with the electromagnetic field. Taking into account both the tree-level diagram and the diagrams with the self-energy insertions into the external legs (i.e. the tree-level diagram times $Z_H - 1$) yields a common factor Z_H which is equal to zero.

We have used free fermion propagators for the quarks given by

$$S_i(k) = \frac{1}{m_i - \not{k}} \quad (2.4)$$

with an effective constituent quark mass m_i .

For calculational convenience we will choose a simple Gaussian form for the vertex function $\bar{\Phi}_H(-k^2)$. The minus sign in the argument of this function is chosen to emphasize that we are working in Minkowski space. One has

$$\bar{\Phi}_H(-k^2) = \exp(k^2/\Lambda_H^2) \quad (2.5)$$

where the parameter Λ_H characterizes the size of the hadron H . Since k^2 turns into $-k_E^2$ in Euclidean space the form (2.5) has the appropriate fall-off behavior in the Euclidean region. We emphasize that any choice for Φ_H is appropriate as long as it falls off sufficiently fast in the ultraviolet region of Euclidean space to render the corresponding Feynman diagrams ultraviolet finite. As mentioned before we shall choose a Gaussian form for Φ_H for calculational convenience.

We have included the confinement of quarks to our model in Ref. [1]. It was done, first, by introducing the scale integration in the space of α -parameters, and, second, by cutting this scale integration on the upper limit which corresponds to an infrared cutoff. In this manner one removes all possible thresholds presented in the initial quark diagram. The cutoff parameter is taken to be the same for all physical processes. We have adjusted other model parameters by fitting the calculated quantities of the basic physical processes to available experimental data.

Let us give the basic features of the infrared confinement in our model. All physical matrix elements are described by the Feynman diagrams which are the convolution of the free quark propagators and vertex functions. Let n , ℓ and m be the number of the propagators, loops and vertices, respectively. In Minkowski space the ℓ -loop diagram will be represented as

$$\begin{aligned} \Pi(p_1, \dots, p_m) &= \int [d^4k]^\ell \prod_{i_1=1}^m \Phi_{i_1+n}(-K_{i_1+n}^2) \prod_{i_3=1}^n S_{i_3}(\tilde{k}_{i_3} + v_{i_3}), \\ K_{i_1+n}^2 &= \sum_{i_2} (\tilde{k}_{i_1+n}^{(i_2)} + v_{i_1+n}^{(i_2)})^2 \end{aligned} \quad (2.6)$$

where the vectors \tilde{k}_i are linear combinations of the loop momenta k_i . The v_i are linear combinations of the external momenta p_i to be specified in the following. The strings of Dirac matrices appearing in the calculation need not concern us since they do not depend on the momenta. The external momenta p_i are all chosen to be ingoing such that one has $\sum_{i=1}^m p_i = 0$.

Using the Schwinger representation of the local quark propagator one has

$$S(k) = (m + \not{k}) \int_0^\infty d\beta e^{-\beta(m^2 - k^2)} \quad (k^2 < m^2).$$

For the vertex functions one takes the Gaussian form. One has

$$\Phi_{i+n}(-K^2) = \exp[\beta_{i+n} K^2] \quad i = 1, \dots, m, \quad (2.7)$$

where the parameters $\beta_{i+n} = s_i = 1/\Lambda_i^2$ are related to the size parameters. The integrand in Eq. (2.6) has a Gaussian form with the exponential $kak + 2kr + R$ where a is $\ell \times \ell$ matrix depending on the parameter β_i , r is the ℓ -vector composed from the external momenta, and R is a quadratic form of the external momenta. Tensor loop integrals are calculated with the help of the differential representation

$$k_i^\mu e^{2kr} = \frac{1}{2} \frac{\partial}{\partial r_{i\mu}} e^{2kr},$$

We have written a FORM [11] program that achieves the necessary commutations of the differential operators in a very efficient way. After doing the loop integrations one obtains

$$\Pi = \int_0^\infty d^n \beta F(\beta_1, \dots, \beta_n),$$

where F stands for the whole structure of a given diagram. The set of Schwinger parameters β_i can be turned into a simplex by introducing an additional t -integration via the identity

$$1 = \int_0^\infty dt \delta(t - \sum_{i=1}^n \beta_i)$$

leading to

$$\Pi = \int_0^\infty dt t^{n-1} \int_0^1 d^n \alpha \delta\left(1 - \sum_{i=1}^n \alpha_i\right) F(t\alpha_1, \dots, t\alpha_n). \quad (2.8)$$

There are altogether n numerical integrations: $(n-1)$ α -parameter integrations and the integration over the scale parameter t . The very large t -region corresponds to the region where the singularities of the diagram with its local quark propagators start appearing. However, as described in [1], if one introduces an infrared cut-off on the upper limit of the t -integration, all singularities vanish because the integral is now convergent for any value of the set of kinematic variables. We cut off the upper integration at $1/\lambda^2$ and obtain

$$\Pi^c = \int_0^{1/\lambda^2} dt t^{n-1} \int_0^1 d^n \alpha \delta\left(1 - \sum_{i=1}^n \alpha_i\right) F(t\alpha_1, \dots, t\alpha_n).$$

By introducing the infrared cut-off one has removed all potential thresholds in the quark loop diagram, i.e. the quarks are never on-shell and are thus effectively confined. We take the cut-off

parameter λ to be the same in all physical processes. The numerical evaluations have been done by a numerical program written in the FORTRAN code.

As a further illustration of the infrared confinement effect relevant to the applications in this paper we consider the case of a scalar one-loop two-point function. One has

$$\Pi_2(p^2) = \int \frac{d^4 k_E}{\pi^2} \frac{e^{-sk_E^2}}{[m^2 + (k_E + \frac{1}{2}p_E)^2][m^2 + (k_E - \frac{1}{2}p_E)^2]}$$

where we have collected all the nonlocal Gaussian vertex form factors in the numerator factor $e^{-sk_E^2}$. Note that the momenta k_E, p_E are Euclidean momenta. Doing the loop integration one obtains

$$\begin{aligned} \Pi_2(p^2) &= \int_0^\infty dt \frac{t}{(s+t)^2} \int_0^1 d\alpha \exp \left[-tz_{\text{loc}} + \frac{st}{s+t} z_1 \right], \\ z_{\text{loc}} &= m^2 - \alpha(1-\alpha)p^2, \quad z_1 = \left(\alpha - \frac{1}{2} \right)^2 p^2. \end{aligned} \quad (2.9)$$

The integral $\Pi_2(p^2)$ can be seen to have a branch point at $p^2 = 4m^2$ because z_{loc} is zero when $\alpha = 1/2$. By introducing a cut-off on the t -integration one obtains

$$\Pi_2^c(p^2) = \int_0^{1/\lambda^2} dt \frac{t}{(s+t)^2} \int_0^1 d\alpha \exp \left[-tz_{\text{loc}} + \frac{st}{s+t} z_1 \right]. \quad (2.10)$$

The one-loop two-point function $\Pi_2^c(p^2)$ Eq.(2.10) can be seen to have no branch point at $p^2 = 4m^2$.

The gauging of the nonlocal Lagrangian in Eq. (2.1) proceeds in a way suggested in Refs. [12, 13] and used before by us (see, for instance, Refs. [14, 15]). In order to guarantee local invariance of the nonlocal Lagrangian in Eq. (2.1) one multiplies each quark field $q(x_i)$ with a gauge field exponential:

$$q_i(x_i) \rightarrow e^{-ie_{q_1} I(x_i, x, P)} q_i(x_i) \quad (2.11)$$

where

$$I(x_i, x, P) = \int_x^{x_i} dz_\mu A^\mu(z). \quad (2.12)$$

The path P connects the end-points of the path integral. One then expands the gauge exponential up to the requisite power of $e_q A_\mu$ needed in the perturbative series. We need to know only the derivatives of the path integral expressions when calculating the perturbative series. Therefore, we use the formalism suggested in [12, 13] which is based on the path-independent definition of the derivative of $I(x, y, P)$:

$$\lim_{dx^\mu \rightarrow 0} dx^\mu \frac{\partial}{\partial x^\mu} I(x, y, P) = \lim_{dx^\mu \rightarrow 0} [I(x + dx, y, P') - I(x, y, P)] \quad (2.13)$$

where the path P' is obtained from P by shifting the end-point x by dx . The definition (2.13) leads to the key rule

$$\frac{\partial}{\partial x^\mu} I(x, y, P) = A_\mu(x) \quad (2.14)$$

which in turn states that the derivative of the path integral $I(x, y, P)$ does not depend on the path P originally used in the definition.

As a result of this rule we are getting the part of the Lagrangian which describes the nonlocal interaction of the hadron, quark and electromagnetic fields to the first order in the electromagnetic charge.

3. B_s -meson

We give below the necessary definitions of the leptonic decay constants, invariant form factors and helicity amplitudes.

The leptonic decay constants of the pseudoscalar and vector mesons are defined by

$$\begin{aligned} N_c g_P \int \frac{d^4 k}{(2\pi)^4 i} \tilde{\Phi}_P(-k^2) \text{tr} \left[O^\mu S_1(k + w_1 p) \gamma^5 S_2(k - w_2 p) \right] &= f_P p^\mu, \quad p^2 = m_P^2, \\ N_c g_V \int \frac{d^4 k}{(2\pi)^4 i} \tilde{\Phi}_V(-k^2) \text{tr} \left[O^\mu S_1(k + w_1 p) \not{\epsilon}_V S_2(k - w_2 p) \right] &= m_V f_V \epsilon_V^\mu, \quad p^2 = m_V^2, \end{aligned} \quad (3.1)$$

where $N_c = 3$ is the number of colors.

Herein our primary subjects are the following matrix elements, which can be expressed via dimensionless form factors:

$$\begin{aligned} &\langle P'_{[\bar{q}_1 q_3]}(p_2) | \bar{q}_2 O^\mu q_1 | P_{[\bar{q}_3 q_2]}(p_1) \rangle = \\ &= N_c g_P g_{P'} \int \frac{d^4 k}{(2\pi)^4 i} \tilde{\Phi}_P \left(-(k + w_{13} p_1)^2 \right) \tilde{\Phi}_{P'} \left(-(k + w_{23} p_2)^2 \right) \\ &\times \text{tr} \left[O^\mu S_1(k + p_1) \gamma^5 S_3(k) \gamma^5 S_2(k + p_2) \right] = F_+(q^2) P^\mu + F_-(q^2) q^\mu, \end{aligned} \quad (3.2)$$

$$\begin{aligned} &\langle P'_{[\bar{q}_1 q_3]}(p_2) | \bar{q}_2 (\sigma^{\mu\nu} q_\nu) q_1 | P_{[\bar{q}_3 q_2]}(p_1) \rangle = \\ &= N_c g_P g_{P'} \int \frac{d^4 k}{(2\pi)^4 i} \tilde{\Phi}_P \left(-(k + w_{13} p_1)^2 \right) \tilde{\Phi}_{P'} \left(-(k + w_{23} p_2)^2 \right) \\ &\times \text{tr} \left[\sigma^{\mu\nu} q_\nu S_1(k + p_1) \gamma^5 S_3(k) \gamma^5 S_2(k + p_2) \right] = \frac{i}{m_1 + m_2} (q^2 P^\mu - q \cdot P q^\mu) F_T(q^2), \end{aligned} \quad (3.3)$$

$$\begin{aligned} &\langle V(p_2, \epsilon_2)_{[\bar{q}_1 q_3]} | \bar{q}_2 O^\mu q_1 | P_{[\bar{q}_3 q_2]}(p_1) \rangle = \\ &= N_c g_P g_V \int \frac{d^4 k}{(2\pi)^4 i} \tilde{\Phi}_P \left(-(k + w_{13} p_1)^2 \right) \tilde{\Phi}_V \left(-(k + w_{23} p_2)^2 \right) \\ &\times \text{tr} \left[O^\mu S_1(k + p_1) \gamma^5 S_3(k) \not{\epsilon}_2^\dagger S_2(k + p_2) \right] \\ &= \frac{\epsilon_V^\dagger}{m_1 + m_2} \left(-g^{\mu\nu} P \cdot q A_0(q^2) + P^\mu P^\nu A_+(q^2) + q^\mu P^\nu A_-(q^2) + i \epsilon^{\mu\nu\alpha\beta} P_\alpha q_\beta V(q^2) \right), \end{aligned} \quad (3.4)$$

$$\begin{aligned}
& \langle V(p_2, \varepsilon_2)_{[\bar{q}_1 q_3]} | \bar{q}_2 (\sigma^{\mu\nu} q_\nu (1 + \gamma^5)) q_1 | P_{[\bar{q}_3 q_2]}(p_1) \rangle = \\
& = N_c g_P g_V \int \frac{d^4 k}{(2\pi)^4 i} \tilde{\Phi}_P \left(-(k + w_{13} p_1)^2 \right) \tilde{\Phi}_V \left(-(k + w_{23} p_2)^2 \right) \\
& \times \text{tr} \left[(\sigma^{\mu\nu} q_\nu (1 + \gamma^5)) S_1(k + p_1) \gamma^5 S_3(k) \not{\varepsilon}_2^\dagger S_2(k + p_2) \right] \\
& = \varepsilon_V^\dagger \left(-(g^{\mu\nu} - q^\mu q^\nu / q^2) P \cdot q a_0(q^2) + (P^\mu P^\nu - q^\mu P^\nu P \cdot q / q^2) a_+(q^2) + i \varepsilon^{\mu\nu\alpha\beta} P_\alpha q_\beta g(q^2) \right).
\end{aligned} \tag{3.5}$$

Here, $P = p_1 + p_2$, $q = p_1 - p_2$, $\varepsilon_2^\dagger \cdot p_2 = 0$, $p_i^2 = m_i^2$. Since there are three sorts of quarks involved in these processes, we introduce the notation with two subscripts $w_{ij} = m_{q_j} / (m_{q_i} + m_{q_j})$ ($i, j = 1, 2, 3$) so that $w_{ij} + w_{ji} = 1$. The form factors defined in Eq. (3.5) satisfy the physical requirement $a_0(0) = a_+(0)$, which ensures that no kinematic singularity appears in the matrix element at $q^2 = 0$. For reference it is useful to relate the form factors we have defined to those used, e.g., in Ref. [16], which are denoted by a superscript c in the following formulae:

$$\begin{aligned}
F_+ &= f_+^c, \quad F_- = -\frac{m_1^2 - m_2^2}{q^2} (f_+^c - f_0^c), \quad F_T = f_T^c, \\
A_0 &= \frac{m_1 + m_2}{m_1 - m_2} A_1^c, \quad A_+ = A_2^c, \quad A_- = \frac{2m_2(m_1 + m_2)}{q^2} (A_3^c - A_0^c), \quad V = V^c, \\
a_0 &= T_2^c, \quad g = T_1^c, \quad a_+ = T_2^c + \frac{q^2}{m_1^2 - m_2^2} T_3^c.
\end{aligned} \tag{3.6}$$

We note in addition that the form factors $A_i^c(q^2)$ satisfy the constraints: $A_0^c(0) = A_3^c(0)$ and

$$2m_2 A_3^c(q^2) = (m_1 + m_2) A_1^c(q^2) - (m_1 - m_2) A_2^c(q^2).$$

It is convenient to express all physical observables through the helicity form factors H_m . The helicity form factors H_m can be expressed in terms of the invariant form factors in the following way (see Refs. [17, 18, 19]):

(a) Spin $S = 0$:

$$\begin{aligned}
H_t &= \frac{1}{\sqrt{q^2}} \{ (m_1^2 - m_2^2) F_+ + q^2 F_- \}, \\
H_\pm &= 0, \\
H_0 &= \frac{2m_1 |\mathbf{p}_2|}{\sqrt{q^2}} F_+.
\end{aligned} \tag{3.7}$$

(b) Spin $S = 1$:

$$H_t = \frac{1}{m_1 + m_2} \frac{m_1 |\mathbf{p}_2|}{m_2 \sqrt{q^2}} \{ (m_1^2 - m_2^2) (A_+ - A_0) + q^2 A_- \},$$

$$\begin{aligned}
H_{\pm} &= \frac{1}{m_1 + m_2} \left\{ -(m_1^2 - m_2^2) A_0 \pm 2m_1 |\mathbf{p}_2| V \right\}, \\
H_0 &= \frac{1}{m_1 + m_2} \frac{1}{2m_2 \sqrt{q^2}} \left\{ -(m_1^2 - m_2^2) (m_1^2 - m_2^2 - q^2) A_0 + 4m_1^2 |\mathbf{p}_2|^2 A_+ \right\},
\end{aligned} \tag{3.8}$$

where $|\mathbf{p}_2| = \lambda^{1/2}(m_1^2, m_2^2, q^2)/(2m_1)$ is the momentum of the outgoing particles in the rest frame of ingoing particle.

The effective Hamiltonian describing the B_s -nonleptonic decays is given by (see, Ref. [20])

$$\begin{aligned}
\mathcal{H}_{\text{eff}} &= -\frac{G_F}{\sqrt{2}} V_{cb} V_{cs}^\dagger \sum_{i=1}^6 C_i Q_i, \\
Q_1 &= (\bar{c}_{a_1} b_{a_2})_{V-A} (\bar{s}_{a_2} c_{a_1})_{V-A}, & Q_2 &= (\bar{c}_{a_1} b_{a_1})_{V-A}, (\bar{s}_{a_2} c_{a_2})_{V-A}, \\
Q_3 &= (\bar{s}_{a_1} b_{a_1})_{V-A} (\bar{c}_{a_2} c_{a_2})_{V-A}, & Q_4 &= (\bar{s}_{a_1} b_{a_2})_{V-A} (\bar{c}_{a_2} c_{a_1})_{V-A}, \\
Q_5 &= (\bar{s}_{a_1} b_{a_1})_{V-A} (\bar{c}_{a_2} c_{a_2})_{V+A}, & Q_6 &= (\bar{s}_{a_1} b_{a_2})_{V-A} (\bar{c}_{a_2} c_{a_1})_{V+A},
\end{aligned} \tag{3.9}$$

where the subscript $V - A$ refers to the usual left-chiral current $O^\mu = \gamma^\mu(1 - \gamma^5)$ and $V + A$ to the usual right-chiral one $O^\mu_+ = \gamma^\mu(1 + \gamma^5)$. The a_i denote the color indices.

We consider the nonleptonic decays of the B_s -meson into $D_s^- D_s^+$, $D_s^- D_s^{*+}$, $D_s^{*-} D_s^+$, $D_s^{*-} D_s^{*+}$ and $J/\psi \phi$. The calculation of the matrix elements is straightforward. It directly leads to the representation corresponding to *naive* factorization.

The widths can be conveniently expressed in terms of the helicity form factors and leptonic decay constants. In the case of the color-allowed decays one has

$$\begin{aligned}
\Gamma(B_s \rightarrow D_s^- D_s^+) &= \frac{G_F^2}{16\pi} \frac{|\mathbf{q}_2|}{m_{B_s}^2} [\lambda_c^{(s)}]^2 \left(C_2^{\text{eff}} m_{D_s} f_{D_s} H_t^{B_s D_s}(m_{D_s}^2) + 2C_6^{\text{eff}} f_{D_s}^{PS} F_S^{B_s D_s}(m_{D_s}^2) \right)^2, \\
\Gamma(B_s \rightarrow D_s^- D_s^{*+}) &= \frac{G_F^2}{16\pi} \frac{|\mathbf{q}_2|}{m_{B_s}^2} [\lambda_c^{(s)}]^2 \left(C_2^{\text{eff}} m_{D_s} f_{D_s} H_t^{B_s D_s^*}(m_{D_s}^2) + 2C_6^{\text{eff}} \frac{m_{B_s} |\mathbf{q}_2|}{m_{D_s^*}} f_{D_s}^{PS} F_{PS}^{B_s D_s^*}(m_{D_s}^2) \right)^2, \\
\Gamma(B_s \rightarrow D_s^{*-} D_s^+) &= \frac{G_F^2}{16\pi} \frac{|\mathbf{q}_2|}{m_{B_s}^2} [\lambda_c^{(s)}]^2 \left(C_2^{\text{eff}} m_{D_s^*} f_{D_s^*} H_0^{B_s D_s^*}(m_{D_s^*}^2) \right)^2, \\
\Gamma(B_s \rightarrow D_s^{*-} D_s^{*+}) &= \frac{G_F^2}{16\pi} \frac{|\mathbf{q}_2|}{m_{B_s}^2} [\lambda_c^{(s)}]^2 (C_2^{\text{eff}} m_{D_s^*} f_{D_s^*})^2 \sum_{i=0,\pm} \left(H_i^{B_s D_s^*}(m_{D_s^*}^2) \right)^2.
\end{aligned} \tag{3.10}$$

Here, $\lambda_c^{(s)} = |V_{cb} V_{cs}^\dagger|$ and $|\mathbf{q}_2|$ is the momentum of the second outgoing particle in the rest frame of B_s -meson. The Wilson coefficients are combined as $C_2^{\text{eff}} = C_2 + \xi C_1 + C_4 + \xi C_3$ and $C_6^{\text{eff}} = C_6 + \xi C_5$, where a color factor $\xi = 1/N_c$ will be suppressed in the numerical calculations according to $1/N_c$ -expansion. Also we do not take into account the annihilation channels which are available for the color-allowed decays.

The width of the color-suppressed $B_s \rightarrow J/\psi \phi$ decay is written as

$$\Gamma(B_s \rightarrow J/\psi \phi) = \frac{G_F}{16\pi} \frac{|\mathbf{q}_2|}{m_{B_s}^2} [\lambda_c^{(s)}]^2 (C_1^{\text{eff}} + C_5^{\text{eff}})^2 (m_{J/\psi} f_{J/\psi})^2 \sum_{i=0,\pm} \left(H_i^{B_s J/\psi}(m_{J/\psi}^2) \right)^2, \tag{3.11}$$

where the Wilson coefficients are combined as $C_1^{\text{eff}} = C_1 + \xi C_2 + C_3 + \xi C_4$ and $C_5^{\text{eff}} = C_5 + \xi C_6$.

The first application of our relativistic quark model with infrared confinement to the description of the physical observables was done in our paper [1]. We have fitted the model parameters to the leptonic and radiative decay constants of both pseudoscalar and vector mesons. Then we have calculated transition form factors and the widths of the Dalitz decays and compared the results with available experimental data. Here we calculate the form factors describing the transitions of the heavy $B(B_s)$ –mesons into the light ones, e.g. π, K, ρ, K^*, ϕ . These quantities are of great interest due to their applications to semileptonic, nonleptonic and rare decays of the B and B_s –mesons. Basically, they are calculated within the light-cone sum rules (LCSR) in the region of large recoils (small transfer momentum squared). Our approach allows one to evaluate the form factors in the full kinematical regions including zero recoil. First, we update the model parameters by fitting them to the leptonic decay constants, see Table 1, and the widths of the radiative decays, see, Table 2. The results of the fit for the values of quark masses, the infrared cutoff and the size parameters are given in Eqs. (3.12), (3.13) and (3.14), respectively.

$$\begin{array}{cccccc}
 m_u & m_s & m_c & m_b & \lambda & \\
 \hline
 0.235 & 0.424 & 2.16 & 5.09 & 0.181 & \text{GeV}
 \end{array} \tag{3.12}$$

$$\begin{array}{cccccccc}
 \Lambda_\pi & \Lambda_K & \Lambda_D & \Lambda_{D_s} & \Lambda_B & \Lambda_{B_s} & \Lambda_{B_c} & \Lambda_\rho & \\
 \hline
 0.87 & 1.04 & 1.47 & 1.57 & 1.88 & 1.95 & 2.42 & 0.61 & \text{GeV}
 \end{array} \tag{3.13}$$

$$\begin{array}{cccccccc}
 \Lambda_\omega & \Lambda_\phi & \Lambda_{J/\psi} & \Lambda_{K^*} & \Lambda_{D^*} & \Lambda_{D_s^*} & \Lambda_{B^*} & \Lambda_{B_s^*} & \\
 \hline
 0.47 & 0.88 & 1.48 & 0.72 & 1.16 & 1.17 & 1.72 & 1.71 & \text{GeV}
 \end{array} \tag{3.14}$$

In Figs. 1-4 we plot our calculated form factors in the entire kinematical region $0 \leq q^2 \leq q_{\text{max}}^2$. For comparison we also show the results obtained in the light-cone sum rules [26]. The figures highlight the wide range of phenomena accessible within our approach.

As was suggested in Ref. [27], one can check how well the form factors satisfy the low recoil relations among them. In Fig. 5 we plot the ratios

$$R_1 = \frac{T_1(q^2)}{V(q^2)}, \quad R_2 = \frac{T_2(q^2)}{A_1(q^2)}, \quad R_3 = \frac{q^2 T_3(q^2)}{m_B^2 A_2(q^2)}. \tag{3.15}$$

which in the symmetry limit should be all of order $1 - (2\alpha_s/(3\pi) \ln(\mu/m_b))$, i.e. near one. One can see that similar to the LCSR form factors, it works reasonably well for R_1 and R_2 but not for R_3 .

It is interesting to compare the behavior of the form factor calculated from the triangle loop-diagram with those from vector-dominance model (VDM). In the case of the $B - \pi$ –transition, one has

$$F_{\text{VDM}}^{B\pi}(q^2) = \frac{F_+^{B\pi}(0)}{m_{B^*}^2 - q^2}.$$

Table 1: Leptonic decay constants f_H (MeV) used in the least-squares fit for our model parameters.

	This work	Other	Ref.		This work	Other	Ref.
f_π	128.7	130.4 ± 0.2	[21, 22]	f_ω	198.5	198 ± 2	[21]
f_K	156.1	156.1 ± 0.8	[21, 22]	f_ϕ	228.2	227 ± 2	[21]
f_D	205.9	206.7 ± 8.9	[21, 22]	$f_{J/\psi}$	415.0	415 ± 7	[21]
f_{D_s}	257.5	257.5 ± 6.1	[21, 22]	f_{K^*}	213.7	217 ± 7	[21]
f_B	191.1	192.8 ± 9.9	[23]	f_{D^*}	243.3	245 ± 20	[25]
f_{B_s}	234.9	238.8 ± 9.5	[23]	$f_{D_s^*}$	272.0	272 ± 26	[25]
f_{B_c}	489.0	489 ± 5	[24]	f_{B^*}	196.0	196 ± 44	[25]
f_ρ	221.1	221 ± 1	[21]	$f_{B_s^*}$	229.0	229 ± 46	[25]

Table 2: Electromagnetic decay widths (keV) used in the least-squares fit for our model parameters.

Process	This work	Data [21]
$\pi^0 \rightarrow \gamma\gamma$	5.06×10^{-3}	$(7.7 \pm 0.4) \times 10^{-3}$
$\eta_c \rightarrow \gamma\gamma$	1.61	1.8 ± 0.8
$\rho^\pm \rightarrow \pi^\pm \gamma$	76.0	67 ± 7
$\omega \rightarrow \pi^0 \gamma$	672	703 ± 25
$K^{*\pm} \rightarrow K^\pm \gamma$	55.1	50 ± 5
$K^{*0} \rightarrow K^0 \gamma$	116	116 ± 10
$D^{*\pm} \rightarrow D^\pm \gamma$	1.22	1.5 ± 0.5
$J/\psi \rightarrow \eta_c \gamma$	1.43	1.58 ± 0.37

The curves are plotted in Fig. 6. One can see that they agree with quite good accuracy. That means the quark loop in some sense contains an information on the B^* -pole.

As an application of the obtained results we evaluate the widths of the B_s -nonleptonic decays. The modes $D_s^- D_s^+$, $D_s^{*-} D_s^+ + D_s^- D_s^{*+}$ and $D_s^{*-} D_s^{*+}$ give the largest contribution to $\Delta\Gamma$ for the $B_s - \bar{B}_s$ system. The mode $J/\psi\phi$ is suppressed by the color factor but it is interesting for the search of CP-violating New-Physics possible effects in the $B_s - \bar{B}_s$ mixing.

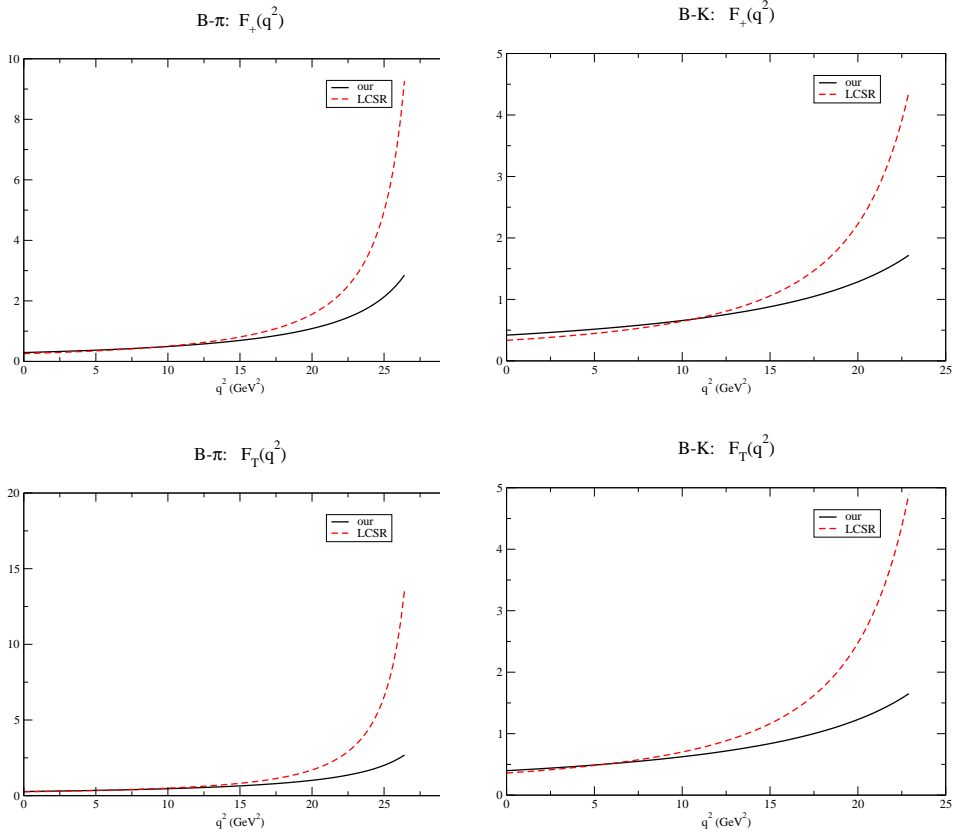


Figure 1: Our results for the form factors appearing in Eqs. (3.2) & (3.3) – *Left panel*, $B - \pi$ –transition; and *right panel*, $B - K$ –transition. For comparison we plot the curves given by LCSR from Ref. [26].

For the CKM-matrix elements we use the values from [21]

$ V_{ud} $	$ V_{us} $	$ V_{ub} $	$ V_{cd} $	$ V_{cs} $	$ V_{cb} $
0.974	0.225	0.00389	0.230	0.975	0.0406

(3.16)

For the Wilson coefficients we take [28]

C_1	C_2	C_3	C_4	C_5	C_6
-0.257	1.009	-0.005	-0.078	0.000	0.001

(3.17)

evaluated to next-to-next-to leading logarithmic accuracy in \overline{MS} (NDR) renormalization scheme at the scale $\mu = 4.8$ GeV [29].

We also need the values of the $B_s - \phi$ –transition evaluated at $q^2 = m_{J/\psi}^2$. We give them in Table 3 and compare with results of Ref. [30].

Finally, we give our results for the branching ratios in Table 4. One can see that there is good agreement with available experimental data.

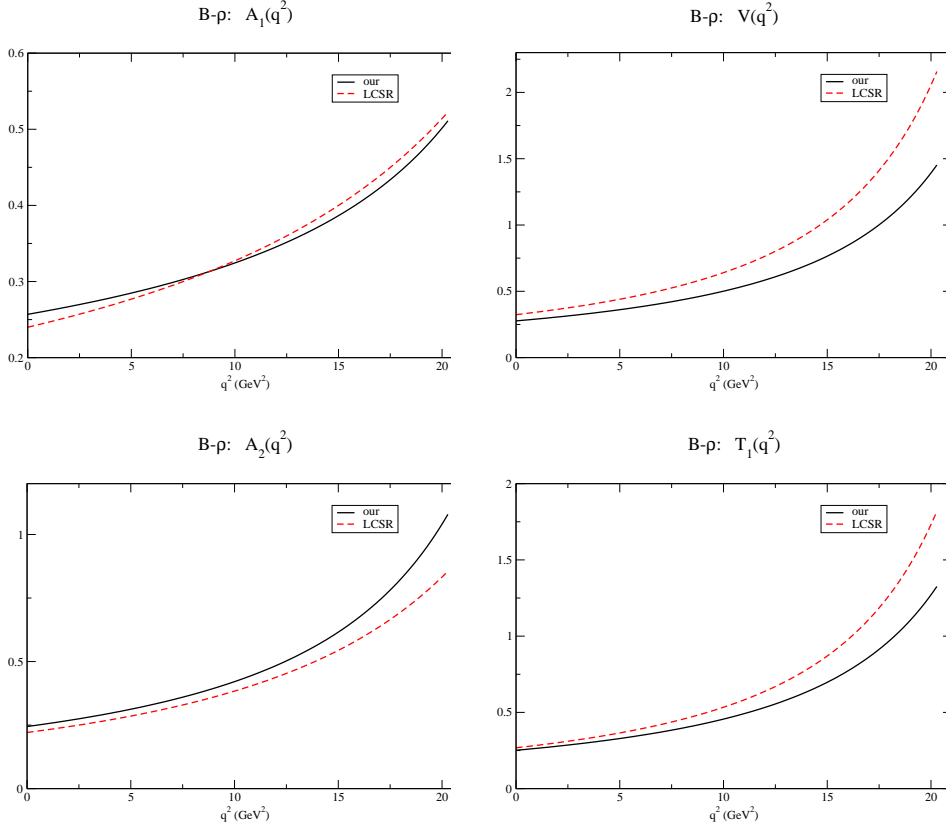


Figure 2: Our results for the form factors appearing in Eqs.(3.4) & (3.5) for $B - \rho$ -transition. For comparison we plot the curves given by LCSR from Ref. [26].

Table 3: The relevant $B_s - \phi$ -form factors at $q^2 = m_{J/\psi}^2$ calculated in our work. For comparison we give the results of Ref. [30].

	This work	Ref. [30]
$A_1(m_{J/\psi}^2)$	0.37	0.42 ± 0.06
$A_2(m_{J/\psi}^2)$	0.48	0.38 ± 0.06
$V(m_{J/\psi}^2)$	0.56	0.82 ± 0.12

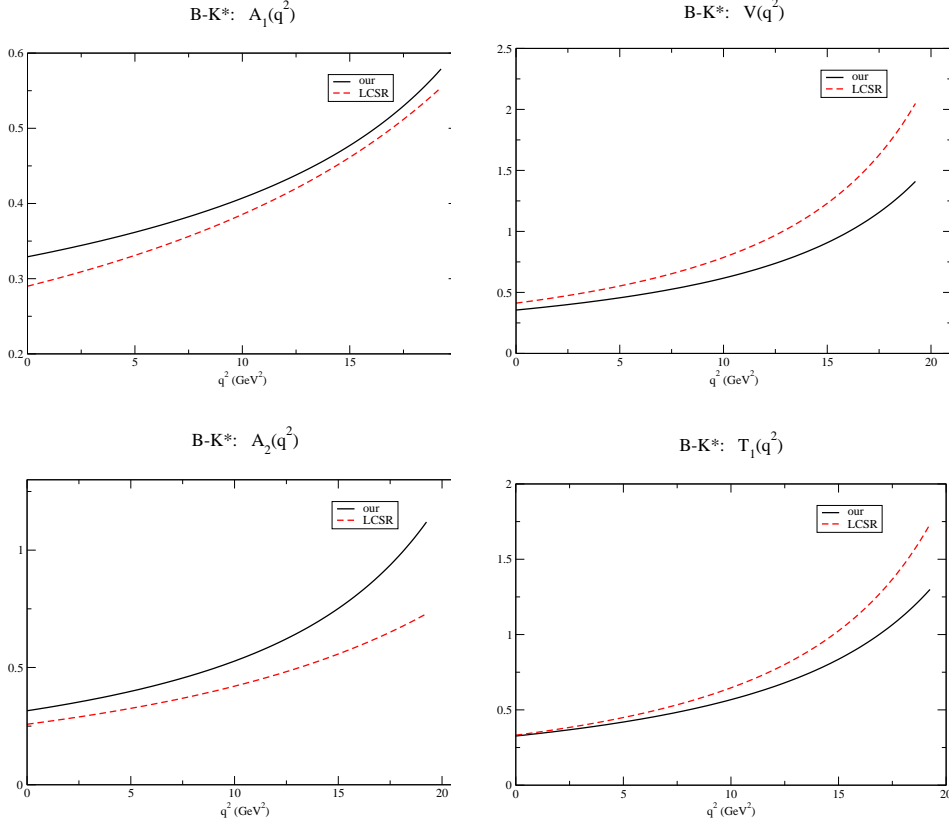


Figure 3: Our results for the form factors appearing in Eqs.(3.4) & (3.5) for $B - K^*$ -transition. For comparison we plot the curves given by LCSR from Ref. [26].

Table 4: Branching ratios (%) of the B_s -nonleptonic decays calculated in our approach.

Process	This work	Data [21]
$B_s \rightarrow D_s^- D_s^+$	1.65	$1.04^{+0.29}_{-0.26}$
$B_s \rightarrow D_s^- D_s^{*+} + D_s^{*-} D_s^+$	2.40	2.8 ± 1.0
$B_s \rightarrow D_s^{*-} D_s^{*+}$	3.18	3.1 ± 1.4
$B_s \rightarrow J/\psi \phi$	0.14	0.14 ± 0.05

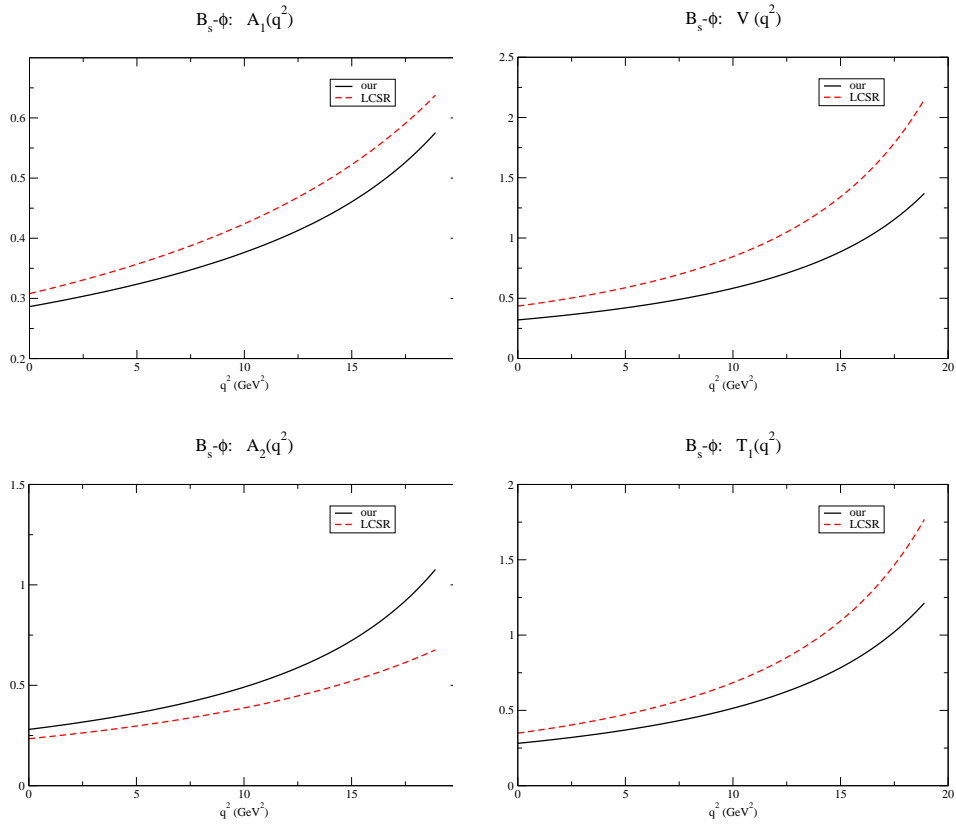


Figure 4: Our results for the form factors appearing in Eqs. (3.4) & (3.5) for $B_s - \phi$ -transition. For comparison we plot the curves given by LCSR from Ref. [26].

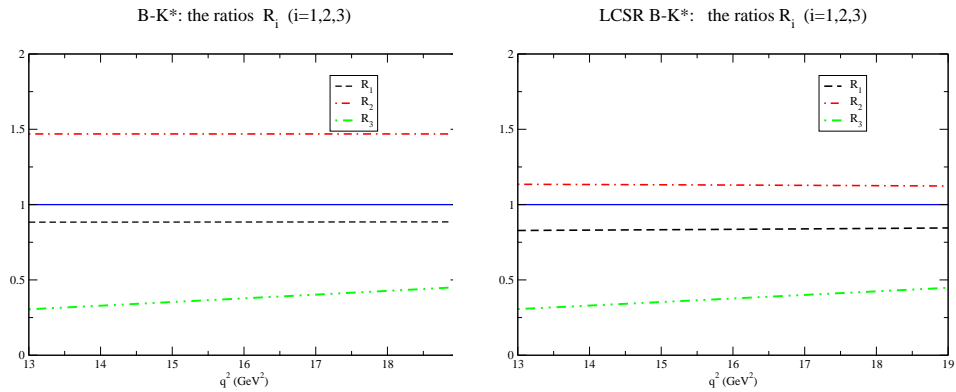


Figure 5: Our results for the ratios of the form factors appearing in Eq. (3.15) for $B - K^*$ -transition.

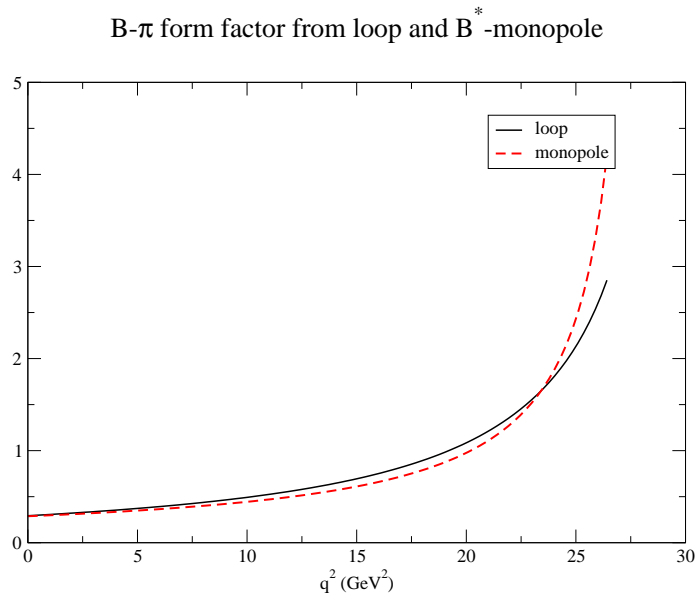


Figure 6: The comparison of the results for the $B-\pi$ form factor obtained on the one hand from the quark-loop diagram and on the another hand from the VDM-monopole.

4. Light baryons

Let us begin our discussion with the proton. The coupling of a proton to its constituent quarks is described by the Lagrangian

$$\mathcal{L}_{\text{int}}^p(x) = g_N \bar{p}(x) \cdot J_p(x) + g_N \bar{J}_p(x) \cdot p(x), \quad (4.1)$$

where we make use of the same interpolating three-quark current $J_p(\bar{J}_p)$ as in Ref. [14]

$$\begin{aligned} J_p(x) &= \int dx_1 \int dx_2 \int dx_3 F_N(x; x_1, x_2, x_3) J_{3q}^{(p)}(x_1, x_2, x_3), \\ J_{3q}^{(p)}(x_1, x_2, x_3) &= \Gamma^A \gamma^5 d^{a_1}(x_1) \cdot [\epsilon^{a_1 a_2 a_3} u^{a_2}(x_2) C \Gamma_A u^{a_3}(x_3)], \\ \bar{J}_p(x) &= \int dx_1 \int dx_2 \int dx_3 F_N(x; x_1, x_2, x_3) \bar{J}_{3q}^{(p)}(x_1, x_2, x_3), \\ \bar{J}_{3q}^{(p)}(x_1, x_2, x_3) &= [\epsilon^{a_1 a_2 a_3} \bar{u}^{a_3}(x_3) \Gamma_A C \bar{u}^{a_2}(x_2)] \cdot \bar{d}^{a_1}(x_1) \gamma^5 \Gamma^A. \end{aligned} \quad (4.2)$$

The matrix $C = \gamma^0 \gamma^2$ is the usual charge conjugation matrix and the a_i ($i = 1, 2, 3$) are color indices. There are two possible kinds of nonderivative three-quark currents: $\Gamma^A \otimes \Gamma_A = \gamma^\alpha \otimes \gamma_\alpha$ (vector current) and $\Gamma^A \otimes \Gamma_A = \frac{1}{2} \sigma^{\alpha\beta} \otimes \sigma_{\alpha\beta}$ (tensor current) with $\sigma^{\alpha\beta} = \frac{i}{2} (\gamma^\alpha \gamma^\beta - \gamma^\beta \gamma^\alpha)$. The interpolating current of the neutron and the corresponding Lagrangian are obtained from the proton case via $p \rightarrow n$ and $u \leftrightarrow d$. As will become apparent later on, one has to consider a general linear superposition of the vector and tensor currents according to

$$J_N = x J_N^T + (1-x) J_N^V, \quad N = p, n \quad (4.3)$$

The electromagnetic vertex function $\Lambda_p^\mu(p, p')$ of the proton consists of four pieces represented by the four two-loop quark diagrams in Fig. 7.

Let us briefly describe a check on the gauge invariance of our calculation. Without gauge invariance there are three independent Lorentz structures in the electromagnetic proton vertex which can be chosen to be

$$\Lambda_p^\mu(p, p') = \gamma^\mu F_1^p(q^2) - \frac{i \sigma^{\mu q}}{2m_N} F_2^p(q^2) + q^\mu F_{NG}^p(q^2), \quad (4.4)$$

where $\sigma^{\mu q} = \frac{i}{2} (\gamma^\mu \gamma^\nu - \gamma^\nu \gamma^\mu) q_\nu$. The form factor $F_{NG}^p(q^2)$ characterizes the non-gauge invariant piece and must therefore vanish for any q^2 in a calculation which respects gauge invariance. For the four contributions of Fig. 2a-2d we found that

$$F_{NGd}^p(q^2) \equiv 0, \quad F_{NGu}^p(q^2) \equiv 0, \quad F_{NG(b)}^p(q^2) \equiv -F_{NG(a)}^p(q^2) \quad \forall q^2. \quad (4.5)$$

It means that the non-gauge invariant contributions of the two vertex diagrams are zero while they vanish for the sum of the two bubble diagrams.

The electromagnetic vertex function of the neutron is obtained from that of the proton by replacing $m_u \leftrightarrow m_d$, $e_u \leftrightarrow e_d$ and $m_p \rightarrow m_n$. $F_1^N(q^2)$ and $F_2^N(q^2)$ are the Dirac and Pauli nucleon form factors which are normalized to the electric charge e_N and anomalous magnetic moment k_N (k_N is given in units of the nuclear magneton $e/2m_p$), respectively, i.e. one has $F_1^N(0) = e_N$ and

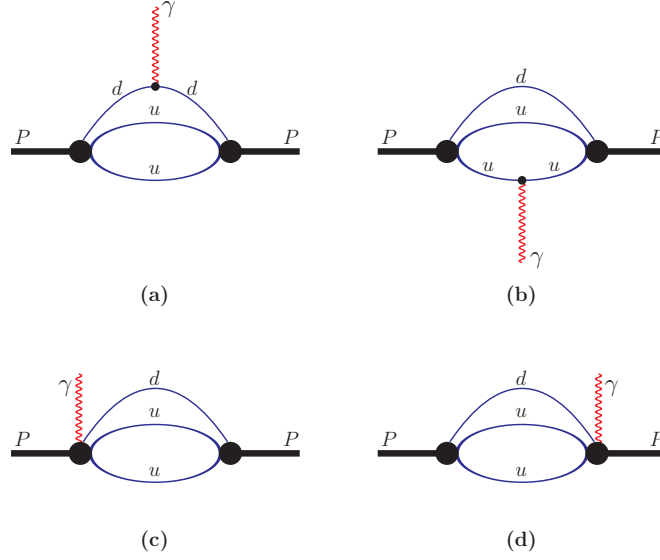


Figure 7: Electromagnetic vertex function of the proton: (a) vertex diagram with the e.m. current attached to d-quark; (b) vertex diagram with the e.m. current attached to u-quark; (c) bubble diagram with the e.m. current attached to the initial state vertex; (d) the bubble diagram with e.m. current attached to the final state vertex.

$F_2^N(0) = k_N$. In particular, one can analytically check by using the integration-by-part identity that the Dirac form factor of the neutron is equal to zero at $q^2 = 0$.

The nucleon magnetic moments $\mu_N = F_1^N(0) + F_2^N(0)$ are known experimentally with high accuracy [21]

$$\mu_p^{\text{expt}} = 2.79 \quad \mu_n^{\text{expt}} = -1.91. \quad (4.6)$$

We will use these values to fit the value of the nucleon size parameter. We obtain

$$\text{vector current} \implies \Lambda_N = 0.36 \text{ GeV} \quad \mu_p = 2.79 \quad \mu_n = -1.70, \quad (4.7)$$

$$\text{tensor current} \implies \Lambda_N = 0.61 \text{ GeV} \quad \mu_p = 2.79 \quad \mu_n = -1.69. \quad (4.8)$$

It is convenient to introduce the Sachs electromagnetic form factors of nucleons

$$G_E^N(q^2) = F_1^N(q^2) + \frac{q^2}{4m_N^2} F_2^N(q^2), \quad G_M^N(q^2) = F_1^N(q^2) + F_2^N(q^2). \quad (4.9)$$

The slopes of these form factors are related to the well-known electromagnetic radii of nucleons:

$$\langle r_E^2 \rangle^N = 6 \frac{dG_N^E(q^2)}{dq^2} \Big|_{q^2=0}, \quad \langle r_M^2 \rangle^N = \frac{6}{G_M^N(0)} \frac{dG_M^N(q^2)}{dq^2} \Big|_{q^2=0}. \quad (4.10)$$

We would like to emphasize that reproducing data on the neutron charge radius $\langle r_E^2 \rangle^n$ is a nontrivial task (see e.g. discussion in Ref.[31]). As well-known the naive nonrelativistic quark model based on SU(6) spin-flavor symmetry implies $\langle r_E^2 \rangle^n \equiv 0$. The dynamical breaking of the

SU(6) symmetry based on the inclusion of the quark spin-spin interaction generates a nonvanishing value of $\langle r_E^2 \rangle^n$. From this point of view the dominant contribution to the $\langle r_E^2 \rangle^n$ comes from the Pauli term:

$$\langle r_E^2 \rangle^n \simeq \frac{6}{4m_N^2} F_2^n(0).$$

The experimental data on the nucleon Sachs form factors in the space-like region $Q^2 = -q^2 \geq 0$ can be approximately described by the dipole approximation

$$G_E^p(q^2) \approx \frac{G_M^p(q^2)}{1 + \mu_p} \approx \frac{G_M^n(q^2)}{\mu_n} \approx \frac{4m_N^2}{q^2} \frac{G_E^n(q^2)}{\mu_n} \approx \frac{1}{(1 - q^2/0.71 \text{ GeV}^2)^2} \equiv D_N(q^2).$$

According to present data the dipole approximation works well up to 1 GeV^2 (with an accuracy of up to 25%). For higher values of Q^2 the deviation of the nucleon form factors from the dipole approximation becomes more pronounced. In particular, the best description of magnetic moments, electromagnetic radii and form factors is achieved when we consider a superposition of the V - and T -currents of nucleons according to Eq. (4.3) with $x = 0.8$. For the size parameter of the nucleon we take $\Lambda_N = 0.5 \text{ GeV}$.

In Table 5 we present the results for the magnetic moments and electromagnetic radii for this set of model parameters. In Fig. 8 we present our results for the q^2 dependence of electromagnetic form factors in the region $Q^2 \in [0, 1] \text{ GeV}^2$. Fig. 8 also shows plots of the dipole approximation to the form factors. The agreement of our results with the dipole approximation is satisfactory. Inclusion of chiral corrections as, for example, developed and discussed in [32] may lead to a further improvement in the low Q^2 description.

Table 5: Electromagnetic properties of nucleons.

Quantity	Our results	Data [21]
μ_p (in n.m.)	2.96	2.793
μ_n (in n.m.)	-1.83	-1.913
r_E^p (fm)	0.805	0.8768 ± 0.0069
$\langle r_E^2 \rangle^n$ (fm ²)	-0.121	-0.1161 ± 0.0022
r_M^p (fm)	0.688	$0.777 \pm 0.013 \pm 0.010$
r_M^n (fm)	0.685	$0.862^{+0.009}_{-0.008}$

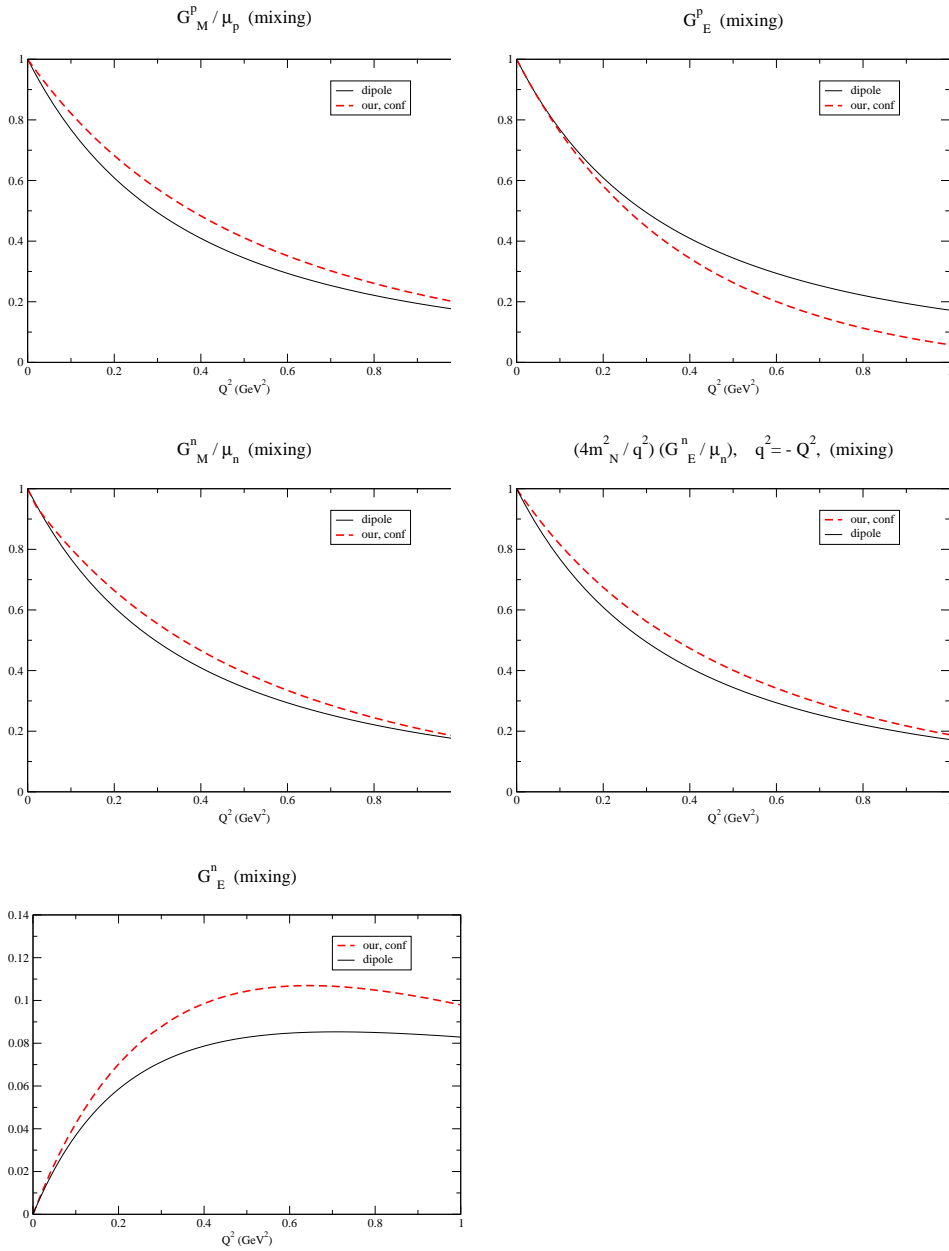


Figure 8: Sachs nucleon form factors in comparisons with the dipole representation in the space-like region $Q \leq 1 \text{ GeV}^2$.

5. The $X(3872)$ -meson as a tetraquark

A narrow charmonium-like state $X(3872)$ was observed in 2003 in the exclusive decay process $B^\pm \rightarrow K^\pm \pi^+ \pi^- J/\psi$ [33]. The $X(3872)$ decays into $\pi^+ \pi^- J/\psi$ and has a mass of $m_X = 3872.0 \pm 0.6(\text{stat}) \pm 0.5(\text{syst})$ very close to the $M_{D^0} + M_{D^{*0}} = 3871.81 \pm 0.25$ mass threshold [21]. Its width was found to be less than 2.3 MeV at 90% confidence level. The state was confirmed in B-decays by the BaBar experiment [34] and in $p\bar{p}$ production by the Tevatron experiments [35].

From the observation of the decay $X(3872) \rightarrow J/\psi \gamma$ reported by [36], it was shown that the only quantum numbers compatible with the data are $J^{PC} = 1^{++}$ or 2^{-+} . However, the observation of the decays into $D^0 \bar{D}^0 \pi^0$ by the Belle and BaBar collaborations [37] allows one to exclude the choice 2^{-+} because the near-threshold decay $X \rightarrow D^0 \bar{D}^0 \pi^0$ is expected to be strongly suppressed for $J = 2$.

The Belle collaboration has reported evidence for the decay mode $X \rightarrow \pi^+ \pi^- \pi^0 J/\psi$ with a strong three-pion peak between 750 MeV and the kinematic limit of 775 MeV [36], suggesting that the process is dominated by the sub-threshold decay $X \rightarrow \omega J/\psi$. It was found that the branching ratio of this mode is almost the same as that of the mode $X \rightarrow \pi^+ \pi^- J/\psi$:

$$\frac{\mathcal{B}(X \rightarrow J/\psi \pi^+ \pi^- \pi^0)}{\mathcal{B}(X \rightarrow J/\psi \pi^+ \pi^-)} = 1.0 \pm 0.4(\text{stat}) \pm 0.3(\text{syst}). \quad (5.1)$$

These observations imply strong isospin violation because the three-pion decay proceeds via an intermediate ω -meson with isospin 0 whereas the two-pion decay proceeds via the intermediate ρ -meson with isospin 1. Also the two-pion decay via the intermediate ρ -meson is very difficult to explain by using an interpretation of the $X(3872)$ as a simple $c\bar{c}$ charmonium state with isospin 0.

There are several different interpretations of the $X(3872)$ in the literature: a molecule bound state ($D^0 \bar{D}^{*0}$) with small binding energy, a tetraquark state composed of a diquark and antidiquark, threshold cusps, hybrids and glueballs. A description of the current theoretical and experimental situation for the new charmonium states may be found in the reviews [38].

We provided in Ref. [2] an independent analysis of the properties of the $X(3872)$ meson which we interpret as a tetraquark state as in [39]. The authors of [39] suggested to consider the $X(3872)$ meson as a $J^{PC} = 1^{++}$ tetraquark state with a symmetric spin distribution: $[cq]_{S=0} [\bar{c}\bar{q}]_{S=1} + [cq]_{S=1} [\bar{c}\bar{q}]_{S=0}$, ($q = u, d$). The nonlocal version of the four-quark interpolating current reads

$$J_{X_q}^\mu(x) = \int dx_1 \dots \int dx_4 \delta\left(x - \sum_{i=1}^4 w_i x_i\right) \Phi_X\left(\sum_{i<j} (x_i - x_j)^2\right) \times \frac{1}{\sqrt{2}} \varepsilon_{abc} \varepsilon_{dec} \left\{ [q_a(x_4) C \gamma^5 c_b(x_1)] [\bar{q}_d(x_3) \gamma^\mu \bar{c}_e(x_2)] + (\gamma^5 \leftrightarrow \gamma^\mu) \right\}, \quad (5.2)$$

where $w_1 = w_2 = m_c/2(m_q + m_c)$ and $w_3 = w_4 = m_q/2(m_q + m_c)$. The matrix $C = \gamma^0 \gamma^2$ is the charge conjugation matrix. The effective interaction Lagrangian describing the coupling of the meson X_q to its constituent quarks is written in the form

$$\mathcal{L}_{\text{int}} = g_X X_{q\mu}(x) \cdot J_{X_q}^\mu(x), \quad (q = u, d). \quad (5.3)$$

The state X_u breaks isospin symmetry maximally so the authors of [39] take the physical states to be a linear superposition of the X_u and X_d states according to

$$X_l \equiv X_{\text{low}} = X_u \cos \theta + X_d \sin \theta,$$

$$X_h \equiv X_{\text{high}} = -X_u \sin \theta + X_d \cos \theta. \quad (5.4)$$

The mixing angle θ can be determined from fitting the ratio of branching ratios Eq. (5.1).

The coupling constant g_X in Eq. (5.3) will be determined from the compositeness condition:

$$Z_X = 1 - \Pi'_X(m_X^2) = 0,$$

where $\Pi_X(p^2)$ is the scalar part of the vector-meson mass operator. The corresponding three-loop diagram describing the X -meson mass operator is shown in Fig. 9.

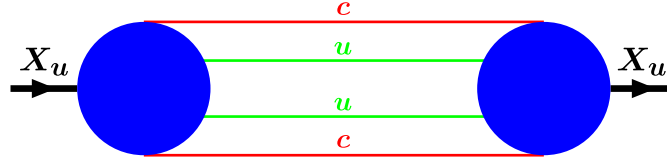


Figure 9: Diagram describing the X_u -meson mass operator.

Next we evaluate the matrix elements of the transitions $X \rightarrow J/\psi + \rho(\omega)$ and $X \rightarrow D + \bar{D}^*$. The relevant Feynman diagrams are shown in Fig. 10.

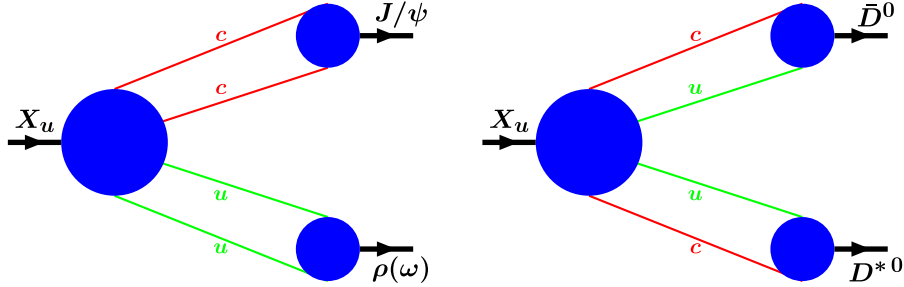


Figure 10: Feynman diagrams describing the decays $X \rightarrow J/\psi + \rho(\omega)$ and $X \rightarrow D + \bar{D}^*$.

Since the $X(3872)$ is very close to the respective thresholds in both cases, the intermediate ρ , ω and D^* mesons have to be treated as off-shell particles. Using the calculated matrix elements for the decay $X \rightarrow J/\psi + \rho(\omega)$ one can evaluate the decay widths $X \rightarrow J/\psi + 2\pi(3\pi)$. We employ the narrow width approximation for this purpose.

There are two new free parameters: the mixing angle θ in Eq. (5.4) and the size parameter Λ_X . We have varied the parameter Λ_X in a large interval and found that the ratio

$$\frac{\Gamma(X_u \rightarrow J/\psi + 3\pi)}{\Gamma(X_u \rightarrow J/\psi + 2\pi)} \approx 0.25$$

is very stable under variations of Λ_X . Hence, by using this result and the central value of the experimental data given in Eq. (5.14), one finds $\theta \approx \pm 18.4^\circ$ for X_l ("+") and X_h ("-"), respectively. This is in agreement with the results obtained in both [39]: $\theta \approx \pm 20^\circ$ and [40]: $\theta \approx \pm 23.5^\circ$. The

decay width is quite sensitive to the change of the size parameter Λ_X . A natural choice is to take a value close to $\Lambda_{J/\psi}$ and Λ_{η_c} which are both around 3 GeV. We have varied the size parameter Λ_X from 2.4 up to 4 GeV and found that the decay width $\Gamma(X \rightarrow J/\psi + n\pi)$ decreases monotonously. This result is in accordance with the experimental bound $\Gamma(X(3872)) \leq 2.3$ MeV and the result obtained in [39]: 1.6 MeV.

In a similar way we calculate the width of the decay $X \rightarrow D^0 \bar{D}^0 \pi^0$ which was observed by the Belle Coll. and reported in [37]. As in the previous case we have varied Λ_X from 2.5 up to 4 GeV and found that the decay width $\Gamma(X_l \rightarrow \bar{D}^0 D^0 \pi^0)$ decreases monotonously. We plot the dependence of the calculated decay widths on the size parameter Λ_X in Fig. 11.

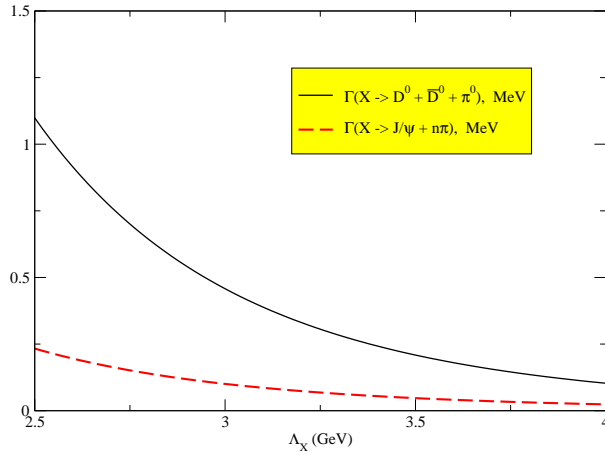


Figure 11: The dependence of the decay widths $\Gamma(X_l \rightarrow \bar{D}^0 D^0 \pi^0)$ and $\Gamma(X \rightarrow J/\psi + n\pi)$ on the size parameter Λ_X .

Using the results of [21], one calculates the experimental rate ratio

$$\frac{\Gamma(X \rightarrow D^0 \bar{D}^0 \pi^0)}{\Gamma(X \rightarrow J/\psi \pi^+ \pi^-)} = 10.5 \pm 4.7 \quad (5.5)$$

The theoretical value for this rate ratio depends only weakly on the size parameter Λ_X :

$$\left. \frac{\Gamma(X \rightarrow D^0 \bar{D}^0 \pi^0)}{\Gamma(X \rightarrow J/\psi \pi^+ \pi^-)} \right|_{\text{theor}} = 4.5 \pm 0.2. \quad (5.6)$$

The theoretical error reflects the Λ_X dependence of the ratio. The ratio lies within the experimental uncertainties given by Eq. (5.5).

The matrix element of the decay $X(3872) \rightarrow J/\psi + \gamma$ can be calculated from the Feynman diagrams shown in Fig. 12.

The invariant matrix element for the decay is given by

$$M(X_q(p) \rightarrow J/\psi(q_1) + \gamma(q_2)) = i(2\pi)^4 \delta^{(4)}(p - q_1 - q_2) \varepsilon_X^\mu \varepsilon_\gamma^\rho \varepsilon_{J/\psi}^\nu T_{\mu\rho\nu}(q_1, q_2) \quad (5.7)$$

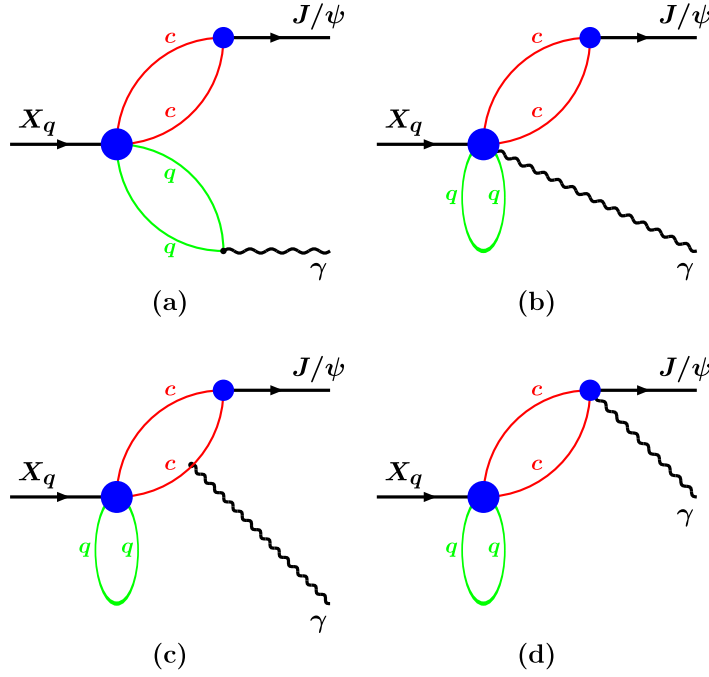


Figure 12: Feynman diagrams describing the decay $X \rightarrow J/\psi + \gamma$.

We have analytically checked on the gauge invariance of the unintegrated transition matrix element by contraction with the photon momentum q_2 which yields $q_2^\rho T_{\mu\rho\nu}(q_1, q_2) = 0$ using the identities

$$S(k_2) \not{q}_2 S(k_2 + q_2) = S(k_2 + q_2) - S(k_2),$$

$$\int_0^1 d\tau \tilde{\Phi}'(-\tau a - (1-\tau)b)(a-b) = \tilde{\Phi}(-b) - \tilde{\Phi}(-a).$$

If one takes the on-mass shell conditions

$$\varepsilon_X^\mu p_\mu = 0, \quad \varepsilon_{J/\psi}^\nu q_{1\nu} = 0, \quad \varepsilon_\gamma^\rho q_{2\rho} = 0 \quad (5.8)$$

into account one can write down five seemingly independent Lorentz structures

$$T_{\mu\rho\nu}(q_1, q_2) = \varepsilon_{q_2\mu\nu\rho} q_1^2 W_1 + \varepsilon_{q_1q_2\nu\rho} q_{1\mu} W_2 + \varepsilon_{q_1q_2\mu\rho} q_{2\nu} W_3 + \varepsilon_{q_1q_2\mu\nu} q_{1\rho} W_4 + \varepsilon_{q_1\mu\nu\rho} q_1 q_2 W_5.$$

Further, using the gauge invariance condition

$$q_2^\rho T_{\mu\rho\nu} = q_1 q_2 \varepsilon_{q_1q_2\mu\nu} (W_4 + W_5) = 0$$

one has $W_4 = -W_5$ which reduces the set of independent covariants to four:

$$T_{\mu\rho\nu}(q_1, q_2) = \varepsilon_{q_2\mu\nu\rho} q_1^2 W_1 + \varepsilon_{q_1q_2\nu\rho} q_{1\mu} W_2 + \varepsilon_{q_1q_2\mu\rho} q_{2\nu} W_3 + \left(\varepsilon_{q_1q_2\mu\nu} q_{1\rho} - q_1 q_2 \varepsilon_{q_1\mu\nu\rho} W_4 \right).$$

The gauge invariance condition $W_4 = -W_5$ provides for a numerical check on the gauge invariance of our calculation as described further on.

However, there are two nontrivial relations among the four covariants which can be derived by noting [46] that the tensor

$$T_{\mu[v_1 v_2 v_3 v_4 v_5]} = g_{\mu v_1} \epsilon_{v_2 v_3 v_4 v_5} + \text{cycl.}(v_1 v_2 v_3 v_4 v_5) \quad (5.9)$$

vanishes in four dimensions since it is totally antisymmetric in the five indices $(v_1, v_2, v_3, v_4, v_5)$. Upon contraction with $q_1^\mu q_1^{v_1} q_2^{v_2}$ and $q_2^\mu q_1^{v_1} q_2^{v_2}$ one finds

$$\begin{aligned} q_1^2 \epsilon_{q_2 \mu \nu \rho} + \epsilon_{q_1 q_2 \nu \rho} q_{1\mu} + \left(\epsilon_{q_1 q_2 \mu \nu} q_{1\rho} - q_1 q_2 \epsilon_{q_1 \mu \nu \rho} \right) &= 0 \\ q_1 q_2 \epsilon_{q_2 \mu \nu \rho} - \epsilon_{q_1 q_2 \nu \rho} q_{1\mu} - \epsilon_{q_1 q_2 \mu \rho} q_{2\nu} &= 0. \end{aligned}$$

It reduces the set of independent covariants to two. This is the appropriate number of independent covariants since the photon transition is described by two independent amplitudes as e.g. by the $E1$ and $M2$ transition amplitudes.

The quantities W_i are represented by the four-fold integrals

$$W_i = \int_0^\infty dt \int_0^1 d^3 \beta F_i(t, \beta_1, \beta_2, \beta_3) \quad (5.10)$$

where we have suppressed the additional dependence of the integrand F_i on the set of variables $p^2, q_1^2, q_2^2; m_q, m_c, s_X, s_{J/\psi}$ with $s_X = 1/\Lambda_X^2$ and $s_{J/\psi} = 1/\Lambda_{J/\psi}^2$. The integrals in Eq. (5.10) have branch points at $p^2 = 4(m_q + m_c)^2$ (diagram in Fig. 12-a) and at $p^2 = 4m_c^2$ (diagrams in Figs. 12-b,c,d). At these points the integrals become divergent in the conventional sense when $t \rightarrow \infty$. Under numerical check on gauge invariance of the amplitude $T_{\mu\rho\nu}(q_1, q_2)$, we assume that the X-meson momentum squared is below the nearest unitarity threshold, i.e. $p^2 < 4m_c^2$. The gauge invariance condition is independent of the overall couplings g_X and $g_{J/\psi}$ and thus the numerical check can be done irrelevant of their values.

In the next step we introduce an infrared cutoff $1/\lambda^2$ on the upper limit of the t-integration in Eq. (5.10). In this manner one removes all possible singularities and thereby guarantees quark confinement. However, the contributions coming from the bubble diagrams in Figs. 12-b,c,d blow up at $p^2 = m_X^2$ compare with the contribution from the diagram in Fig. 12-a. The bubble diagrams are needed only to guarantee the gauge invariance of the matrix element. For physical applications one should take into account only the gauge invariant part of the diagram in Fig. 12-a.

It is convenient to present the decay width via helicity or multipole amplitudes. One has

$$\Gamma(X \rightarrow J/\psi + \gamma) = \frac{1}{12\pi} \frac{|\mathbf{q}_2|}{m_X^2} \left(|H_L|^2 + |H_T|^2 \right) = \frac{1}{12\pi} \frac{|\mathbf{q}_2|}{m_X^2} \left(|A_{E1}|^2 + |A_{M2}|^2 \right) \quad (5.11)$$

where the helicity amplitudes H_L and H_T are expressed in terms of the Lorentz amplitudes as

$$\begin{aligned} H_L &= im_X m_{J/\psi} |\mathbf{q}_2| \left[W_1 + \frac{m_X}{m_{J/\psi}^2} |\mathbf{q}_2| W_3 - W_4 \right], \\ H_T &= -im_{J/\psi}^2 |\mathbf{q}_2| \left[W_1 + \frac{m_X}{m_{J/\psi}^2} |\mathbf{q}_2| W_2 - \left(1 + \frac{m_X |\mathbf{q}_2|}{m_{J/\psi}^2} \right) W_4 \right], \\ |\mathbf{q}_2| &= \frac{m_X^2 - m_{J/\psi}^2}{2m_X}. \end{aligned} \quad (5.12)$$

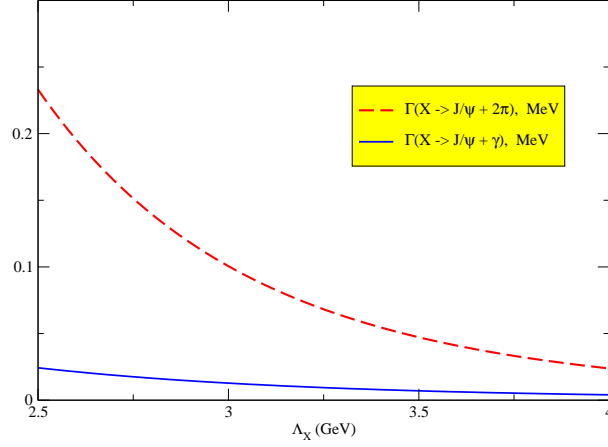


Figure 13: The dependence of the decay widths $\Gamma(X_l \rightarrow J/\psi + \gamma)$ and $\Gamma(X_l \rightarrow J/\psi + 2\pi)$ on the size parameter Λ_X .

Proceeding in a such way one will get the dependence of the decay widths $\Gamma(X_l \rightarrow J/\psi + \gamma)$ and $\Gamma(X_l \rightarrow J/\psi + 2\pi)$ plotted in Fig. 13.

Note that the radiative decay width for $X_h = -X_u \sin \theta + X_d \cos \theta$ is almost an order of magnitude less than for $X_l = X_u \cos \theta + X_d \sin \theta$. If one takes $\Lambda_X \in (3, 4)$ GeV with the middle point $\Lambda_X = 3.5$ GeV then the ratio of the widths is equal to

$$\frac{\Gamma(X_l \rightarrow J/\psi + \gamma)}{\Gamma(X_l \rightarrow J/\psi + 2\pi)} \Big|_{\text{theor}} = 0.15 \pm 0.03 \quad (5.13)$$

which fits very well the experimental data from the BELLE collaboration written down in their Eq. (5.14).

$$\frac{\Gamma(X \rightarrow J/\psi + \gamma)}{\Gamma(X \rightarrow J/\psi + 2\pi)} = \begin{cases} 0.14 \pm 0.05 & \text{BELLE [41]} \\ 0.22 \pm 0.06 & \text{BABAR [42]} \end{cases} \quad (5.14)$$

The last topic which we would like to discuss is the impact of the intermediate X-resonance on the value of the J/ψ -dissociation cross section, see [43]-[44]. The relevant s-channel diagram is shown in Fig. 14.

We take $\Gamma_X = 1$ MeV in the Breit-Wigner propagator and set $\Lambda_X = 3.5$ GeV when calculating the matrix elements. We plot the behavior of the relevant cross sections in Fig. 15. One can see that in the case of charged D-mesons (left panel in Fig. 15) the maximum value of the cross section is about 0.32 mb at $E = 3.88$ GeV. This result should be compared with the result of the cross section $\sigma(J/\psi + \pi \rightarrow D + \bar{D}^*) \approx 0.9$ mb at $E = 4.0$ GeV, see, [45] and the result of the cross section $\sigma(J/\psi + \rho \rightarrow D + \bar{D}^*) \approx 2.9$ mb at $E = 3.9$ GeV, see, [43]. Thus the X-resonance gives a sizable contribution to the J/ψ -dissociation cross section. It would be interesting to do a complete analysis of the J/ψ dissociation cross section in view of our new results on the s-channel contribution of the X(3872) tetraquark state.

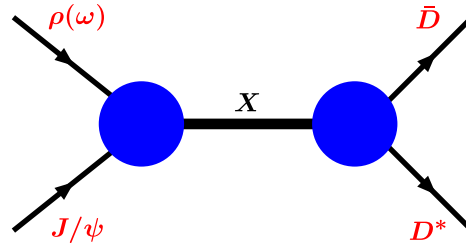


Figure 14: Diagram describing the X-resonance contribution to the J/ψ -dissociation process.

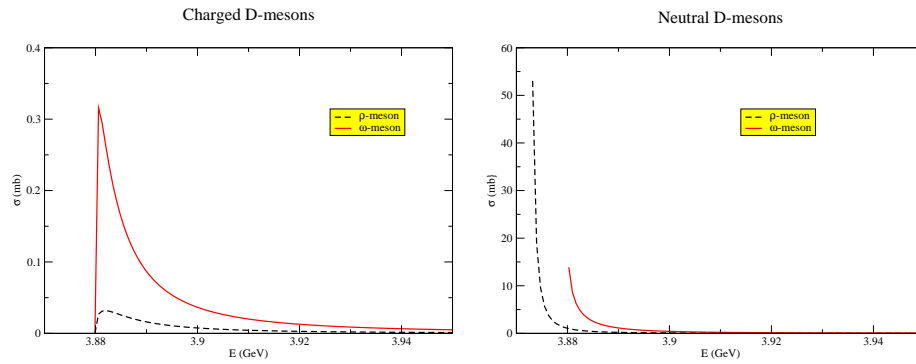


Figure 15: The cross sections of the processes $J/\psi + \nu^0 \rightarrow X \rightarrow D + D^*$. Charged D-mesons– left panel, neutral D-mesons–right panel.

6. Summary

- We have presented a refined covariant quark model which includes infrared confinement of quarks.
- We have calculated the transition form factors of the heavy B_s -meson to light pseudoscalar and vector mesons, which are needed as ingredients for the calculation of the semileptonic, nonleptonic, and rare decays. Our form factor results hold in the full kinematical range of momentum transfer.
- We have made use of the calculated form factors to calculate the nonleptonic decays $B_s \rightarrow D_s \bar{D}_s, \dots$ and $B_s \rightarrow J/\psi \phi$, which have been widely discussed recently in the context of $B_s - \bar{B}_s$ -mixing and CP violation.
- We have applied our approach to baryon physics by using the same values of the constituent quark masses and infrared cutoff as in meson sector.
- We have calculated the nucleon magnetic moments and charge radii and also electromagnetic form factors at low energies.
- The properties of the $X(3872)$ as a tetraquark have been studied in the framework of a covariant quark model with infrared confinement.
- The matrix elements of the off-shell transitions $X \rightarrow J/\psi + \rho(\omega)$ and $X \rightarrow D + \bar{D}^*$ were calculated.
- The obtained results were then used to evaluate the widths of the experimentally observed decays $X \rightarrow J/\psi + 2\pi(3\pi)$ and $X \rightarrow D^0 + \bar{D}^0 + \pi^0$.
- The possible impact of the $X(3872)$ on the J/ψ -dissociation process was discussed.
- We have calculated the matrix element of the transition $X \rightarrow \gamma + J/\psi$ and have shown its gauge invariance. We have evaluated the $X \rightarrow \gamma + J/\psi$ decay width and the polarization of the J/ψ in the decay.
- The comparison with available experimental data allows one to conclude that the $X(3872)$ can be a tetraquark state.

References

- [1] T. Branz, A. Faessler, T. Gutsche, M. A. Ivanov, J. G. Körner and V. E. Lyubovitskij, Phys. Rev. D **81** (2010) 034010 [arXiv:0912.3710 [hep-ph]].
- [2] S. Dubnicka, A. Z. Dubnickova, M. A. Ivanov and J. G. Körner, Phys. Rev. D **81** (2010) 114007 [arXiv:1004.1291 [hep-ph]].
- [3] S. Dubnicka, A. Z. Dubnickova, M. A. Ivanov, J. G. Körner and G. G. Saidullaeva, AIP Conf. Proc. **1343** (2011) 385 [arXiv:1011.4417 [hep-ph]].

- [4] S. Dubnicka, A. Z. Dubnickova, M. A. Ivanov, J. G. Koerner, P. Santorelli and G. G. Saidullaeva, Phys. Rev. D **84** (2011) 014006 [arXiv:1104.3974 [hep-ph]].
- [5] T. Gutsche, M. A. Ivanov, J. G. Körner, V. E. Lyubovitskij and P. Santorelli, Phys. Rev. D **86** (2012) 074013 [arXiv:1207.7052 [hep-ph]].
- [6] S. Weinberg, Phys. Rev. **130** (1963) 776.
- [7] A. Salam, Nuovo Cim. **25** (1962) 224.
- [8] K. Hayashi, M. Hirayama, T. Muta, N. Seto and T. Shirafuji, Fortsch. Phys. **15** (1967) 625.
- [9] G. V. Efimov and M. A. Ivanov, Int. J. Mod. Phys. A **4** (1989) 2031.
- [10] G. V. Efimov and M. A. Ivanov, *The Quark Confinement Model of Hadrons*, (IOP Publishing, Bristol & Philadelphia, 1993).
- [11] J. A. M. Vermaseren, Nucl. Phys. Proc. Suppl. **183** (2008) 19 [arXiv:0806.4080 [hep-ph]]; arXiv:math-ph/0010025.
- [12] S. Mandelstam, Annals Phys. **19** (1962) 1.
- [13] J. Terning, Phys. Rev. D **44** (1991) 887.
- [14] M. A. Ivanov, M. P. Locher and V. E. Lyubovitskij, Few Body Syst. **21** (1996) 131.
- [15] A. Faessler, T. Gutsche, M. A. Ivanov, J. G. Körner, V. E. Lyubovitskij, D. Nicmorus and K. Pumsa-ard, Phys. Rev. D **73** (2006) 094013. [hep-ph/0602193].
- [16] A. Khodjamirian, T. Mannel, N. Offen, Phys. Rev. **D75** (2007) 054013. [hep-ph/0611193].
- [17] M. A. Ivanov, J. G. Körner and P. Santorelli, Phys. Rev. D **63** (2001) 074010. [arXiv:hep-ph/0007169].
- [18] M. A. Ivanov, J. G. Körner and P. Santorelli, Phys. Rev. D **71** (2005) 094006. [arXiv:hep-ph/0501051].
- [19] M. A. Ivanov, J. G. Körner, P. Santorelli, Phys. Rev. **D73** (2006) 054024. [hep-ph/0602050].
- [20] G. Buchalla, A. J. Buras, M. E. Lautenbacher, Rev. Mod. Phys. **68** (1996) 1125 [hep-ph/9512380].
- [21] J. Beringer et al. (Particle Data Group), Phys. Rev. D **86** (2012) 010001.
- [22] J. L. Rosner, S. Stone, “*Leptonic Decays of Charged Pseudoscalar Mesons*,” [arXiv:1002.1655 [hep-ex]].
- [23] J. Laiho, E. Lunghi, R. S. Van de Water, Phys. Rev. **D81** (2010) 034503 [arXiv:0910.2928 [hep-ph]].
- [24] T. -W. Chiu *et al.* [TWQCD Collaboration], Phys. Lett. **B651** (2007) 171 [arXiv:0705.2797 [hep-lat]].
- [25] D. Becirevic, P. Boucaud, J. P. Leroy, V. Lubicz, G. Martinelli, F. Mescia, F. Rapuano, Phys. Rev. **D60** (1999) 074501 [hep-lat/9811003].
- [26] P. Ball and R. Zwicky, Phys. Rev. D **71** (2005) 014029 [arXiv:hep-ph/0412079]; Phys. Rev. **D71** (2005) 014029 [hep-ph/0412079].
- [27] C. Bobeth, G. Hiller, D. van Dyk, JHEP **1007** (2010) 098 [arXiv:1006.5013 [hep-ph]]; JHEP **1107** (2011) 067 [arXiv:1105.0376 [hep-ph]].
- [28] W. Altmannshofer, P. Ball, A. Bharucha, A. J. Buras, D. M. Straub, M. Wick, JHEP **0901** (2009) 019 [arXiv:0811.1214 [hep-ph]].
- [29] C. Bobeth, M. Misiak, J. Urban, Nucl. Phys. **B574** (2000) 291 [hep-ph/9910220].

- [30] S. Faller, R. Fleischer, T. Mannel, Phys. Rev. **D79** (2009) 014005 [arXiv:0810.4248 [hep-ph]].
- [31] W. R. B. de Araujo, T. Frederico, M. Beyer and H. J. Weber, Int. J. Mod. Phys. A **18** (2003) 5767 [hep-ph/0305120].
- [32] A. Faessler, T. Gutsche, V. E. Lyubovitskij and K. Pumsard, Phys. Rev. D **73** (2006) 114021 [hep-ph/0511319].
- [33] S. K. Choi *et al.* [Belle Collaboration], Phys. Rev. Lett. **91** (2003) 262001.
- [34] B. Aubert *et al.* [BaBar Collaboration], Phys. Rev. Lett. **93** (2004) 041801.
- [35] D. E. Acosta *et al.* [CDF Collaboration], Phys. Rev. Lett. **93** (2004) 072001; V. M. Abazov *et al.* [D0 Collaboration], Phys. Rev. Lett. **93** (2004) 162002; T. Aaltonen, *et al.* [CDF Collaboration], Phys. Rev. Lett. **103** (2009) 152001.
- [36] K. Abe *et al.*, [Belle Collaboration], [arXiv:hep-ex/0505037,hep-ex/0505038]; B. Aubert *et al.* [BaBar Collaboration], Phys. Rev. D **74** (2006) 071101; A. Abulencia *et al.* [CDF Collaboration], Phys. Rev. Lett. **98** (2007) 132002.
- [37] G. Gokhroo *et al.* [Belle Collaboration], Phys. Rev. Lett. **97** (2006) 162002; B. Aubert *et al.* [BaBar Collaboration], Phys. Rev. D **77** (2008) 011102.
- [38] E. Eichten, S. Godfrey, H. Mahlke and J. L. Rosner, Rev. Mod. Phys. **80** (2008) 1161; S. Godfrey and S. L. Olsen, Ann. Rev. Nucl. Part. Sci. **58** (2008) 51; M. B. Voloshin, Prog. Part. Nucl. Phys. **61** (2008) 455.
- [39] L. Maiani, F. Piccinini, A. D. Polosa and V. Riquer, Rev. D **71** (2005) 014028.
- [40] F. S. Navarra and M. Nielsen, Phys. Lett. B **639** (2006) 272 [arXiv:hep-ph/0605038].
- [41] K. Abe *et al.* [Belle Collaboration], [hep-ex/0505037].
- [42] E. Klempt and A. Zaitsev, Phys. Rept. **454**, 1 (2007) [arXiv:0708.4016 [hep-ph]].
- [43] T. Barnes, “Charmonium cross sections and the QGP,” arXiv:nucl-th/0306031.
- [44] D. Blaschke, arXiv:0912.4479 [hep-ph];
- [45] M. A. Ivanov, J. G. Körner and P. Santorelli, Phys. Rev. D **70**, 014005 (2004) [arXiv:hep-ph/0311300];
- [46] J. G. Körner, M. C. Mauser, Lect. Notes Phys. **647** (2004) 212 [hep-ph/0306082].